Target Tracking using Signal Strength Differences for Long-Range IoT Networks

Li, Xuhong; Abou Nasa, Mohamad; Rezaei, Farshid; Tufvesson, Fredrik

Published in:
8th IEEE ICC Workshop on Advances in Network Localization and Navigation (ANLN), 2020

DOI:
10.1109/ICCWorkshops49005.2020.9145373

2020

Document Version:
Peer reviewed version (aka post-print)

Target Tracking using Signal Strength Differences for Long-Range IoT Networks

[1]Xuhong Li, Mohamad Abou Nasa, Farshid Rezaei, [1]Fredrik Tufvesson
[1]Department of Electrical and Information Technology, Lund University, Sweden.
Email: {xuhong.li, fredrik.tufvesson}@eit.lth.se

***Abstract*—Radio based positioning or tracking solutions typically require wideband signals or phase coherent antennas. In this paper, we present a target tracking method based on received non-coherent signal strength differences (RSSDs) between antennas for outdoor Internet-of-things (IoT) scenarios. We introduce an RSSD model based on classical path-loss models. With known antenna patterns and antenna array geometries, the RSSD model enables direct mapping between RSSD and angle of arrival, without involving parameters like transmit power, path-loss coefficient, etc. The RSSD model is then exploited in a recursive Bayesian filtering method for target tracking where a particle filter-based implementation is used. The performance is evaluated using outdoor measurements in a low-power wide area network (LoRaWAN) based IoT system. Besides, we also investigate the potential of the RSSD model for AoA estimation. The experimental results show the capability of the proposed framework for real-time target/AoA tracking; reasonable accuracy is achieved even when using non-averaged RSS measurements and under non line-of-sight (NLoS) conditions. Furthermore, the non-coherent approach has low computational complexity, scales well, and is flexible to allow for different antenna array configurations.**

I. Introduction

Location-awareness is a key enabler for various emerging applications related to the Internet-of-things (IoT). Numerous existing commercial systems and research prototypes for localization in IoT scenarios build upon features like time-of-arrival (ToA), angle-of-arrival (AoA), received signal strength (RSS), etc. Among these, RSS-based localization is especially appealing due to its simplicity and broad support for many low-cost technologies, for instance radio frequency identification (RFID), Bluetooth Low Energy, and LoRa [1], with a working range from a few meters up to several kilometers. In this work, we focus on RSS-based localization methods, with particular interest in the middle to long-range outdoor IoT scenarios.

To formulate the localization problem, connected IoT devices are classified as anchor nodes with known locations, and a target node of which the location is to be determined. RSS-based localization and tracking solutions are typically based on proximity, fingerprinting [2], [3] and ranging [4] methods. Fingerprinting-based localization exploits the unique structure of RSS spatial distribution by matching position-labeled RSS measurements with the pre-acquired measurements (fingerprints) at the positions of interest. The performance is influenced by the density of fingerprints and degrades in dynamic scenarios. RSS-based ranging for localization is another common approach. By exploiting a path-loss model (PLM) [5], it is possible to map the RSS measurement to a range estimate, which is further used to infer the target location w.r.t. the anchor coordinates. RSS-based ranging can be unreliable under the conditions of imperfect knowledge about source transmit power, path-loss coefficient, environmental influence, etc. Moreover, it should be noted that long-range IoT systems normally use very high receiver sensitivity for extending the coverage range, but very low bandwidth and packet rate. This means that when tracking a moving target, sufficient RSS samples are often not available to average out small scale fading. Typically, RSS-based ranging for outdoor IoT localization solutions provide accuracies from one to a few hundred meters [6], [7]. Instead of directly using RSS, localization approaches are proposed to use differences between RSS measurements (RSSDs) obtained at, e.g., consecutive sampling steps [8], different anchors [9], [10], or adjacent antennas at each anchor [11]. However, most of them are dedicated to short-range and indoor scenarios.

In this work, each anchor node is assumed to be equipped with an antenna array of known geometry and antenna pattern. On the basis of the PLM, we introduce an RSSD model, which enables direct mapping between the AoAs and the RSSD measurements obtained from non-coherent antennas, without involving parameters like transmit power, path-loss coefficient, etc. The RSSD model is then exploited in a recursive Bayesian filter for target tracking or AoA estimation. Experimental results using outdoor LoRaWAN based measurements show that real-time outdoor target tracking using RSSD measurements is possible even with non-averaged measurements under NLoS conditions. Besides, the proposed framework has good generality, scales well with different antenna array configurations, and is compatible with different IoT technologies.

The rest of the paper is structured as follows: Section II introduces the RSSD model and problem formulation. Section III presents the RSSD-based tracking algorithms. Experimental results are given in Section IV. Section V concludes the paper.

II. Problem Overview

We consider the case that a target node is equipped with a single antenna and has unknown time-varying positions $\boldsymbol{p}_k = [p_{\mathrm{x},k},\, p_{\mathrm{y},k}]^{\mathrm{T}} \in \mathbb{R}^{2\times 1}$, $k = 1, \cdots, K$. In the area of interest, J anchor nodes are distributed with known positions $\boldsymbol{c}_j \in \mathbb{R}^{2\times 1}$ and known array orientations ϕ_j, $j \in \mathcal{J} \triangleq \{1, \cdots, J\}$. Each anchor node has N_j directional antennas indexed with $i \in \mathcal{N}_j \triangleq \{1, \cdots, N_j\}$ and the angular separation between adjacent antennas is β, as depicted in Fig. 1.

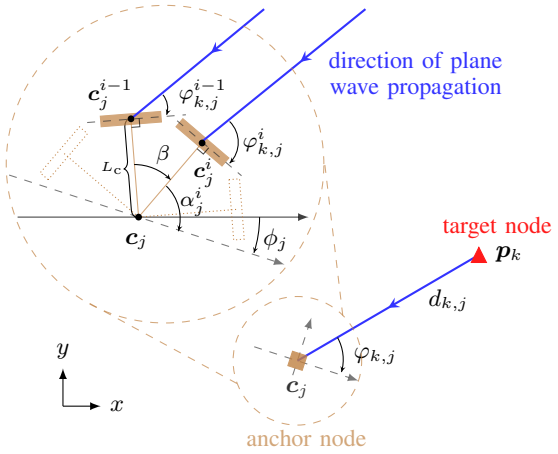

Fig. 1: An exemplary antenna array structure equipped at an anchor node.

The anchor position $\boldsymbol{c}_j$ refers to the center of the array, or more precisely the intersection point of perpendicular lines to antennas' surfaces. The target node is assumed to be the transmitter, and anchor nodes to be the receivers, but with some straightforward modifications, it can work in the opposite direction as well. At time k, AoA $\varphi_{k,j}$ and the propagation distance[1] $d_{k,j}$ from the target to the jth anchor are defined as $\varphi_{k,j} = \angle(\boldsymbol{p}_k - \boldsymbol{c}_j) + \phi_j$ and $d_{k,j} = \|\boldsymbol{p}_k - \boldsymbol{c}_j\|$, $\|\cdot\|$ is the Euclidean norm. With known distance L_c from antenna phase center $\boldsymbol{c}_j^i$ to $\boldsymbol{c}_j$, and the orientation α_j^i of the ith antenna w.r.t. the local coordinate system of jth anchor, the propagation distance $d_{k,j}^i$ and AoA $\varphi_{k,j}^i$ w.r.t. ith antenna are easily calculated as $d_{k,j}^i = \sqrt{L_\mathrm{c}^2 + (d_{k,j})^2 - 2L_\mathrm{c} d_{k,j} \cos\beta_{k,j}^i}$ and $\varphi_{k,j}^i = \varphi_{k,j} + \frac{\pi}{2} - \alpha_j^i$, where the angle $\beta_{k,j}^i$ is given as $\beta_{k,j}^i = |\varphi_{k,j} - \alpha_j^i|$ and $|\cdot|$ is the absolute value, Here, we define the domain $\varphi_{k,j} \in [0^\circ \sim 180^\circ]$ as the positive array direction, $\varphi_{k,j} \in (180^\circ \sim 360^\circ)$ as the negative array direction.

A. RSS model

At time k, the instantaneous received RSS (in dBm) at the ith antenna of jth anchor can be generally expressed as

$$P_{k,j}^i = P_0 + G_\mathrm{Rx}(\varphi_{k,j}^i) - 10\eta \log_{10}\left(\frac{d_{k,j}^i}{d_0}\right) + S_{\mathrm{L},k,j}^i + S_{\mathrm{S},k,j}^i, \tag{1}$$

according to the PLM [5]. The first term on the right side P_0 accounts for the transmit power P_Tx (in dBm), the transmit antenna gain G_Tx and the path loss $L_\mathrm{ref}(d_0)$ at the reference distance $d_0 = 1\,\mathrm{m}$, i.e., $P_0 = P_\mathrm{Tx} + G_\mathrm{Tx} + L_\mathrm{ref}(d_0)$. Furthermore, η is the path-loss coefficient, $G_\mathrm{Rx}(\varphi_{k,j}^i)$ is the receive antenna gain, $S_{\mathrm{L},k,j}^i$ models the position-dependent shadowing term, which is slowly varying over time. The last term $S_{\mathrm{S},k,j}^i$ models the random and fast variations of RSS in time or space, of which the impact is normally reduced by averaging over multiple samples that are consecutively received within a certain time duration.

RSS-based ranging for localization based on (1) can be problematic. P_Tx is typically unknown to receivers, and may vary slowly with battery drain over time. Unknown device orientation leads to the variation of G_Tx. η is closely related to the specific characteristics of the environment. As common practice, those parameters are either simultaneously estimated at each time instance, or precomputed from measurements. Under far-field propagation conditions, the parameters P_Tx, G_Tx and η can be assumed as the same for the antennas at each anchor node. Besides, the position-dependent slow fading process $S_{\mathrm{L},k,j}^i$ are highly correlated over adjacent antennas. Inspired by the arguments above, the difference between RSSs measured at adjacent antennas can be described by a much simpler model than (1), which excludes those unknown but common parameters.

B. RSSD model

Based on (1), the RSSD measurement between two antennas of the jth anchor node at time k is modeled as

$$\begin{aligned} P_{\Delta,k,j}^{(a,b)} &= P_{k,j}^a - P_{k,j}^b \\ &= G_{\Delta,k,j}^{(a,b)}(\varphi_{k,j}) + D_{k,j}^{(a,b)} + \omega_{k,j}^{(a,b)}, \end{aligned} \tag{2}$$

where $\{a, b\} \in \mathcal{N}_j$, and $a < b$. The first term on the right side $G_{\Delta,k,j}^{(a,b)}(\varphi_{k,j})$ represents the antenna gain difference, given as

$$G_{\Delta,k,j}^{(a,b)}(\varphi_{k,j}) = G_\mathrm{Rx}(\varphi_{k,j}^a) - G_\mathrm{Rx}(\varphi_{k,j}^b). \tag{3}$$

The second term $D_{k,j}^{(a,b)} = 10\eta \log_{10} \frac{d_{k,j}^b}{d_{k,j}^a}$ in (2) involves the propagation distances and path-loss coefficient. The last term $\omega_{k,j}^{(a,b)}$ accounts for the difference between two independent fast fading processes, the difference between two highly correlated slow fading processes, as well as hardware-related impairments. Fig. 2 shows simulated values of $D_{k,j}^{(a,b)}$ by assuming $\eta = 3.5$ and $\beta = 45^\circ$. It can be observed that given a constant AoA $\varphi_{k,j}$, the value of $D_{k,j}^{(a,b)}$ drops to under 1 dB after 5 m and continuously converges to 0 dB with distance $d_{k,j}$ increasing. Since we focus on scenarios where the distance $d_{k,j}$ is at least a few tens of meters, $D_{k,j}^{(a,b)}$ has a negligible impact on $P_{\Delta,k,j}^{(a,b)}$ compared to the other two terms in (2). Hence, the model (2) can be further simplified as

$$P_{\Delta,k,j}^{(a,b)} \triangleq G_{\Delta,k,j}^{(a,b)}(\varphi_{k,j}) + \omega_{k,j}^{(a,b)}. \tag{4}$$

An experimental measurement is performed to test how the simplified model works. Two directional antennas shown in Fig. 5b are placed in the middle of the open field (IV-A1) with the angular separation $\beta = 45^\circ$ and one wavelength distance between phase centers. RSS samples are measured every 5° in the angular domain $\varphi_{k,j} \in [0^\circ \sim 360^\circ)$ while keeping $d_{k,j} = 20\,\mathrm{m}$. As shown in Fig. 3, the measured RSSDs with/without averaging match well with the predicted RSSD values $G_{\Delta,k,j}^{(a,b)}(\varphi_{k,j})$ in the positive array direction. In the negative array direction, the measured RSSDs show a similar but noisier pattern as $G_{\Delta,k,j}^{(a,b)}(\varphi_{k,j})$. We also noticed that one

[1]We assume that the propagation condition from the target to each anchor is either line-of-sight (LoS) or obstructed LOS (OLoS), hence the propagation distance could be approximately given as the norm product.

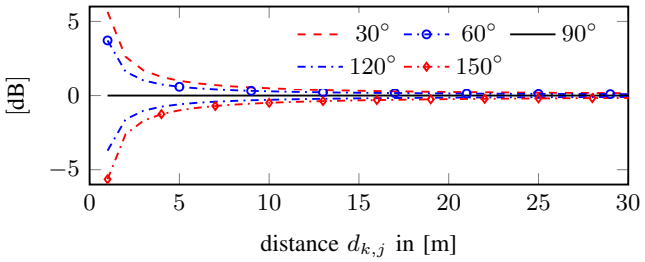

Fig. 2: Experimental values of $D_{k,j}^{(a,b)}$ as a function of varying distance $d_{k,j}$ while keeping constant AoA $\varphi_{k,j}$.

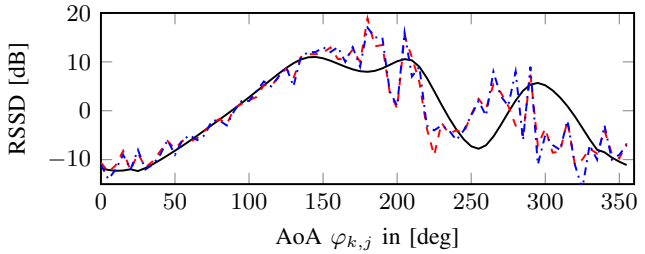

Fig. 3: Comparison of ground truth RSSD $G_{\Delta,k,j}^{(a,b)}$ (——) and measured RSSDs $P_{\Delta,k,j}^{(a,b)}$: RSS samples are averaged at each AoA (- - -); one RSS sample is used at each AoA (-·-·-).

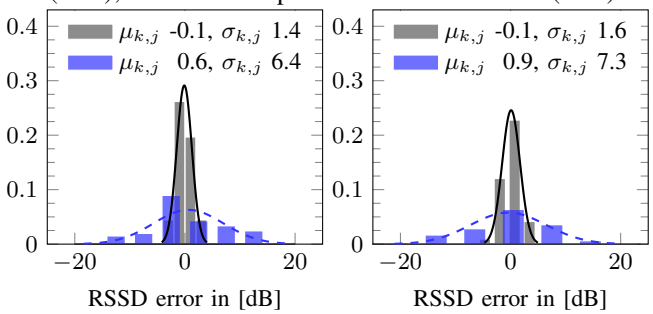

(a) (b)

Fig. 4: Empirical density of RSSD errors $|P_{\Delta,k,j}^{(a,b)} - G_{\Delta,k,j}^{(a,b)}|$. (a) samples are averaged at each AoA, (b) one sample is used at each AoA. Array positive direction: ▭, negative direction: ▭.

RSSD value is not uniquely mapped to one AoA, meaning that the posterior distribution of the AoA given one RSSD measurement can be multimodal. However, fusing RSSD measurements from more than one antenna pair and anchors would lead to a unimodal distribution. According to the empirical density of RSSD errors shown in Fig. 4, $\omega_{k,j}^{(a,b)}$ approximately follows a Gaussian process, i.e., $\omega_{k,j}^{(a,b)} \sim \mathcal{N}(\mu_{k,j}, \sigma_{k,j}^2)$, with the mean $\mu_{k,j}$ close to zero.

C. Target Tracking and AoA Estimation Problems

In reality, it is possible that at some time instances only a subset of antennas of each anchor, i.e., $\mathcal{N}'_{k,j}$ and $\mathcal{N}'_{k,j} \subseteq \mathcal{N}_j$, provide valid RSS measurements. At time k, we assume that at least two antennas at each anchor provide RSS measurements, i.e., $\text{card}\{\mathcal{N}'_{k,j}\} \geq 2$, $\text{card}\{\cdot\}$ represents the cardinality of a set. The RSSD measurements at the jth anchor are given as $\boldsymbol{z}_{k,j} = [z_{k,j}^1, \ldots, z_{k,j}^{l_{j,k}}, \ldots, z_{k,j}^{L_{j,k}}]^{\mathrm{T}}$, with $l_{j,k} \in \mathcal{L}_{j,k} \triangleq \{1, \cdots, L_{j,k}\}$. Each RSSD measurement $z_{k,j}^{l_{j,k}}$ is obtained by taking the differences between RSS measurements from antenna pairs with adjacent indexes, for instance $\{a_{l_{j,k}}, b_{l_{j,k}}\} \in \mathcal{N}'_{k,j}$, and $a_{l_{j,k}} < b_{l_{j,k}}$. Hence, the number of RSSD measurements $L_{j,k} = \text{card}\{\mathcal{N}'_{k,j}\} - 1$ is time variant. By stacking the vectors $\boldsymbol{z}_{k,j}$ from all anchors, we have the full measurement vector at time k, $\boldsymbol{z}_k = [\boldsymbol{z}_{k,1}^{\mathrm{T}}, \ldots, \boldsymbol{z}_{k,j}^{\mathrm{T}}, \ldots, \boldsymbol{z}_{k,J}^{\mathrm{T}}]^{\mathrm{T}}$.

As a proof-of-concept work, we investigate the potential of the proposed RSSD model in two aspects: i) tracking the target node $\boldsymbol{p}_k$ by fusing all the past and current measurements from all anchors $\boldsymbol{z}_{1:k} = [\boldsymbol{z}_1^{\mathrm{T}}, \ldots, \boldsymbol{z}_k^{\mathrm{T}}]^{\mathrm{T}}$; ii) recursively estimating the AoA $\varphi_{k,j}$ using RSSD measurements from a single anchor, $\boldsymbol{z}_{1:k,j} = [\boldsymbol{z}_{1,j}^{\mathrm{T}}, \ldots, \boldsymbol{z}_{k,j}^{\mathrm{T}}]^{\mathrm{T}}$. The reason to bring up the second aspect is that AoA estimates can potentially be fused with existing ranging features, such as the TDoA in LoRaWAN, to enhance outdoor IoT localization.

III. RSSD-based Tracking Algorithms

A. Target Tracking

1) State Space and Measurement Model: The state space vector of the target at time k is given by $\boldsymbol{x}_k = [\boldsymbol{p}_k^{\mathrm{T}}, \Delta\boldsymbol{p}_k^{\mathrm{T}}]^{\mathrm{T}} \in \mathbb{R}^{4\times 1}$, where the vector $\Delta\boldsymbol{p}_k = [\Delta p_{\mathrm{x},k}, \Delta p_{\mathrm{y},k}]^{\mathrm{T}} \in \mathbb{R}^{2\times 1}$ contains the change rates of the target position $\boldsymbol{p}_k$. The agent state evolves according to a first-order Markov process. The evolution of the state $\boldsymbol{x}_k$ is described by the state-transition probability density function (pdf) $f(\boldsymbol{x}_k|\boldsymbol{x}_{k-1})$, which is defined by a linear, near constant-velocity model [12, Section 6.3.2], i.e.,

$$\boldsymbol{x}_k = \boldsymbol{F}\boldsymbol{x}_{k-1} + \boldsymbol{\Gamma}\boldsymbol{n}_k, \tag{5}$$

where the state transition matrix $\boldsymbol{F} \in \mathbb{R}^{4\times 4}$ and $\boldsymbol{\Gamma} \in \mathbb{R}^{4\times 2}$ are given as

$$\boldsymbol{F} = \begin{bmatrix} 1 & 0 & \Delta T & 0 \\ 0 & 1 & 0 & \Delta T \\ 0 & 0 & \Delta T & 0 \\ 0 & 0 & 0 & \Delta T \end{bmatrix}, \quad \boldsymbol{\Gamma} = \begin{bmatrix} \frac{\Delta T^2}{2} & 0 \\ 0 & \frac{\Delta T^2}{2} \\ \Delta T & 0 \\ 0 & \Delta T \end{bmatrix}. \tag{6}$$

Here, ΔT is the update rate, $\boldsymbol{n}_k \in \mathbb{R}^{2\times 1}$ is the driving process that is independent and identically distributed (iid) across k, zero-mean and Gaussian with covariance matrix $\sigma_{\mathrm{n}}^2\boldsymbol{I}_2$. $\boldsymbol{I}_2$ represents the 2×2 identity matrix. The corresponding measurement model which describes the non-linear mapping from state vector to an RSSD measurement is defined as

$$z_{k,j}^{l_{j,k}} = G_{\Delta,k,j}^{(a_{l_{j,k}}, b_{l_{j,k}})}(\boldsymbol{x}_k) + \omega_{l_{j,k}}, \tag{7}$$

where $G_{\Delta,k,j}^{(a_{l_{j,k}}, b_{l_{j,k}})}(\boldsymbol{x}_k)$ represents the nonlinear mapping from the hidden state $\boldsymbol{x}_k$ to an RSSD observation described in (3), and $\omega_{l_{j,k}}$ is iid across $l_{j,k}$, j and k, zero-mean and Gaussian with variance σ_{g}^2.

2) Recursive Bayesian Filtering: The estimation of the target state $\boldsymbol{x}_k$ is formulated as a Bayesian filtering problem, where the posterior pdf $f(\boldsymbol{x}_k|\boldsymbol{z}_{1:k})$ is recursively obtained in two stages: prediction and update. The prediction step is based on the Chapman-Kolmogorov equation [13]

$$f(\boldsymbol{x}_k|\boldsymbol{z}_{1:k-1}) = \int f(\boldsymbol{x}_k|\boldsymbol{x}_{k-1}) f(\boldsymbol{x}_{k-1}|\boldsymbol{z}_{1:k-1}) \mathrm{d}\boldsymbol{x}_{k-1}, \tag{8}$$

and an update step is performed based on Bayes' rule

$$f(\boldsymbol{x}_k|\boldsymbol{z}_{1:k}) = \frac{f(\boldsymbol{z}_k|\boldsymbol{x})f(\boldsymbol{x}_k|\boldsymbol{z}_{1:k-1})}{f(\boldsymbol{z}_k|\boldsymbol{z}_{1:k-1})} \tag{9}$$

given the measurement at time k. Assuming that the measurement $z_{k,j}^{l_{j,k}}$ is conditionally independent across $l_{j,k}$ and j given the target state $\boldsymbol{x}_k$, the likelihood function $f(\boldsymbol{z}_k|\boldsymbol{x}_k)$ is factorized as

$$f(\boldsymbol{z}_k|\boldsymbol{x}_k) = \prod_{j=1}^{J}\prod_{l_{j,k}=1}^{L_{j,k}} f(z_{k,j}^{l_{j,k}}|\boldsymbol{x}_k), \tag{10}$$

where

$$f(z_{k,j}^{l_{j,k}}|\boldsymbol{x}_k) = \frac{1}{\sqrt{2\pi\sigma_{\mathrm{g}}^2}}\exp\Big\{-\frac{(z_{k,j}^{l_{j,k}} - G_{\Delta,k,j}^{(a_{l_{j,k}},b_{l_{j,k}})}(\boldsymbol{x}_k))^2}{2\sigma_{\mathrm{g}}^2}\Big\}. \tag{11}$$

An estimate of the target state $\boldsymbol{x}_k$ is then provided by the minimum mean-square error (MMSE) estimator [14], given as

$$\hat{\boldsymbol{x}}_k^{\mathrm{MMSE}} \triangleq \int \boldsymbol{x}_k f(\boldsymbol{x}_k|\boldsymbol{z}_{1:k})\mathrm{d}\boldsymbol{x}_k. \tag{12}$$

3) Particle-Based Implementation: A sequential Monte Carlo (particle-based) implementation [15] is used to realize the recursive Bayesian filtering process, where the prediction and update steps are formulated in an approximate manner. The posterior pdf $f(\boldsymbol{x}_k|\boldsymbol{z}_{1:k})$ is represented by a finite set of particles and corresponding weights, $\{(\bar{\boldsymbol{x}}_k^m, \bar{w}_k^m)\}_{m=1}^M$. Here, M is the number of particles and the weights sum to one, i.e., $\sum_{m=1}^M \bar{w}_k^m = 1$. At time k, the particles are predicted by simply passing the filtered particles at time $k-1$ through the system dynamics as shown in (6), yielding

$$\bar{\boldsymbol{x}}_k^m \sim f(\bar{\boldsymbol{x}}_k^m|\bar{\boldsymbol{x}}_{k-1}^m). \tag{13}$$

Then in the measurement update step, the weights $\bar{w}_k^m$ are computed according to (10), i.e., $\bar{w}_k^m = f(\boldsymbol{z}_k|\bar{\boldsymbol{x}}_k^m)$, and normalized as $\bar{w}_k^m = \bar{w}_k^m / \sum_{m=1}^M \bar{w}_k^m$. Two more steps are introduced after measurement update, i.e., resampling and regularization, to counteract particle degeneracy and impoverishment effects. The reader is referred to [13], [15] for more details. The posterior pdf can be approximated as $f(\boldsymbol{x}_k|\boldsymbol{z}_{1:k}) \approx \sum_{m=1}^M \bar{w}_k^m K(\boldsymbol{x}_k - \bar{\boldsymbol{x}}_k^m)$ where $K(\cdot)$ denotes the regularization Gaussian Kernel. An approximation of the MMSE state estimate (12) is calculated according to

$$\hat{\boldsymbol{x}}_k^{\mathrm{MMSE}} \approx \sum_{m=1}^{M} \bar{w}_k^m \bar{\boldsymbol{x}}_k^m. \tag{14}$$

The four steps are iterated after setting $k = k+1$.

At time $k = 1$, the particles are initialized by drawing samples $\bar{\boldsymbol{x}}_1^m$ from the prior pdf $f(\boldsymbol{x}_1|\boldsymbol{z}_1) \equiv f(\boldsymbol{x}_1)$. Two situations are considered here: i) *no-prior*: if no informative prior pdf $f(\boldsymbol{x}_1)$ is available, a 2-D uniform distribution with zero center and radius σ_p is used to initialize $\bar{\boldsymbol{p}}_1^m$, and for the position change rate, we use $\{\Delta\bar{p}_{\mathrm{x},1}^m, \Delta\bar{p}_{\mathrm{y},1}^m\} \sim \mathcal{U}(-\sigma_{\Delta p}, \sigma_{\Delta p})$; ii) *noisy-prior*: if noisy information of the ground truth start position $\boldsymbol{p}_1$ is given, $\bar{\boldsymbol{x}}_1^m$ follows a 2-D uniform distribution with radius σ_p' and center $\boldsymbol{p}_1$.

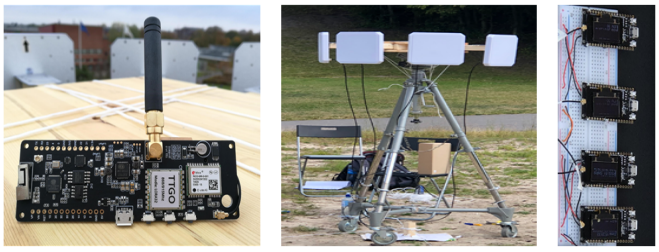

(a) (b) (c)

Fig. 5: Experimental measurement setup: (a) target node: TTGO T-Beam ESP32 module. (b) anchor node 1: four 9 dBi circular antennas are used, and each antenna is connected to a TTGO-LORA32 gateway shown in (c).

B. AoA Estimation

The AoA estimation problem is solved by following the same steps given in III-A. A few minor differences in the formulation are presented here. The AoA state vector is given as $\boldsymbol{x}_k = [\varphi_{k,j}, \Delta\varphi_{k,j}]^{\mathrm{T}} \in \mathbb{R}^{2\times 1}$, where $\Delta\varphi_{k,j}$ is the change rate of $\varphi_{k,j}$. Accordingly, the sizes of the matrices in (5) should be adjusted, more details can be found in [12]. Only measurements from the jth anchor are involved in the likelihood function calculation in (10). We assume no prior pdf $f(\boldsymbol{x}_1)$ is available, hence the particles are initialized from a uniform distribution $\bar{\varphi}_{1,j}^m \sim \mathcal{U}(-\pi, \pi)$ and $\Delta\bar{\varphi}_{1,j}^m \sim \mathcal{U}(-\sigma_\varphi, \sigma_\varphi)$.

IV. Experimental Results

A. Measurement Setup

A LoRaWAN network [1] is used in our experimental setup, where a single-hop link is established between the target node and the gateways. The gateways are connected to a network server via standard IP protocols, and act as bidirectional relays to convert between RF packets and IP packets. The data like GPS "ground truth" and RSS values are decoded in the network server. As shown in Fig. 5, the target node is equipped with an omnidirectional antenna and the transmit power is 14 dBm. Two anchor nodes are used, which are equipped with four and three directional antennas respectively, i.e., $N_1 = 4$ and $N_2 = 3$. The positive array directions are pointing to the target moving areas. The distance between the phase centers of two adjacent antennas is one wavelength, and the angular separation is $\beta = 45°$. One of the receive antenna beam patterns is measured and assumed to be the same for the rest of the antennas. The maximum spreading factor 12 is used to achieve the longest range, however at the cost of low data rate. The system is operating at the carrier frequency 868 MHz, with a bandwidth of 125 kHz. The gateways are listening to several different channels, every 6 seconds one packet is received at each antenna.

The measurement campaign was performed in two different outdoor scenarios, which are described as follows:

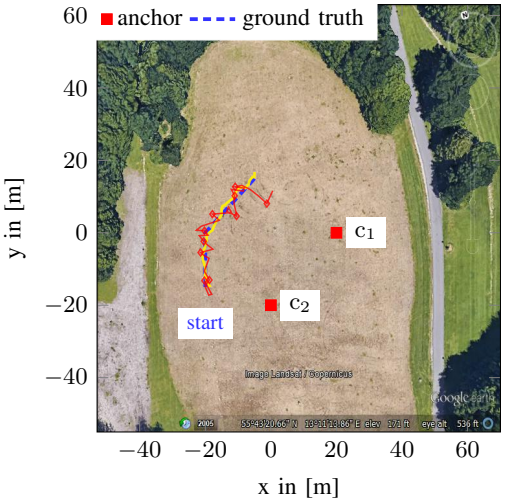

Fig. 6: Target tracking results for open field datasets: *open field-ave* + *no-prior* (——); *open field-one* + *no-prior* (——). Background map: © 2019 Google

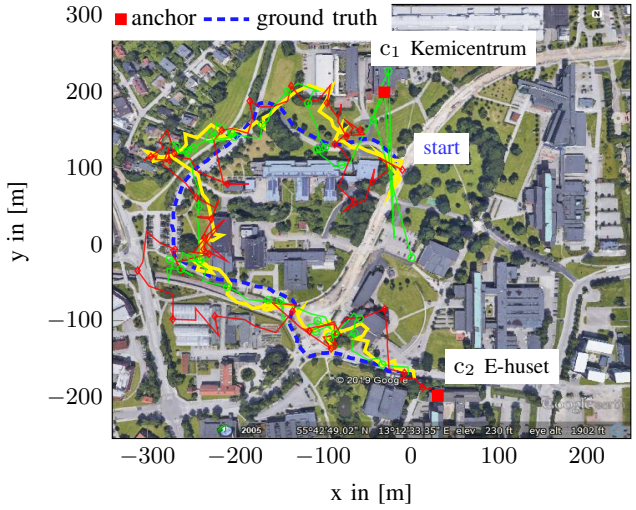

Fig. 7: Target tracking results for urban datasets: *urban-ave* + *noisy-prior* (——); *urban-ave* + *no-prior* (——); *urban-one* + *noisy-prior* (——). Background map: © 2019 Google

1) LoRa open field: The first scenario is an open field surrounded by rich vegetation in Sankt Hans backar, Lund, as shown in Fig. 6. The target node and two anchor nodes are placed at the same height about 1.5 m above the ground. LoS condition is satisfied and measurements are received at all antennas during the whole measurement time. In total, RSS measurements are collected at $K = 38$ sample positions, and the distance inbetween is 1 m. At each position, around five RSS samples are measured at each antenna. Parameters used in the tracking algorithms are: $M = 2000$, $\Delta T = 1$ s, $\sigma_p = 40$ m and $\sigma_{\Delta p} = 1.5$ m/s, $\sigma_\varphi = 3$ degree/s, $\sigma_{\mathrm{g}} = 2.5$ dB.

2) LoRa urban: The second scenario is the campus of Lund University, Sweden, as shown in Fig. 7. Two anchor nodes are placed on two building roofs, which are around 20 m above the ground. The target node is carried by a person walking along a predefined trajectory at a speed around 1 m/s. Every 6 seconds, the movement is paused and we collect around three samples at each antenna. At a few positions, only a subset of antennas provide valid RSS measurements. In total, we have $K = 120$ sample positions. The decoded GPS data from the network server is used as ground truth. Parameters used in the tracking algorithms are: $M = 2000$, $\Delta T = 1$ s, $\sigma_p = 400$ m, $\sigma_{\Delta p} = 7$ m/s, $\sigma'_p = 50$ m, $\sigma_\varphi = 5$ degree/s, and $\sigma_{\mathrm{g}} = 3.6$ dB.

Using the measured RSS samples, we generate two type of datasets for performance evaluation: i) *open field-ave* and *urban-ave*: multiple RSS samples collected from the same antenna at each position are averaged; ii) *open field-one* and *urban-one*: only one RSS sample of each antenna is used.

B. Results

1) Target tracking: Fig. 8 and Fig. 9 present the target position estimation errors and corresponding empirical cumulative distribution functions (CDFs). For the open field scenario, even without a prior information, the tracking algorithm gives a good initial estimate at $k = 1$ with/without measurement

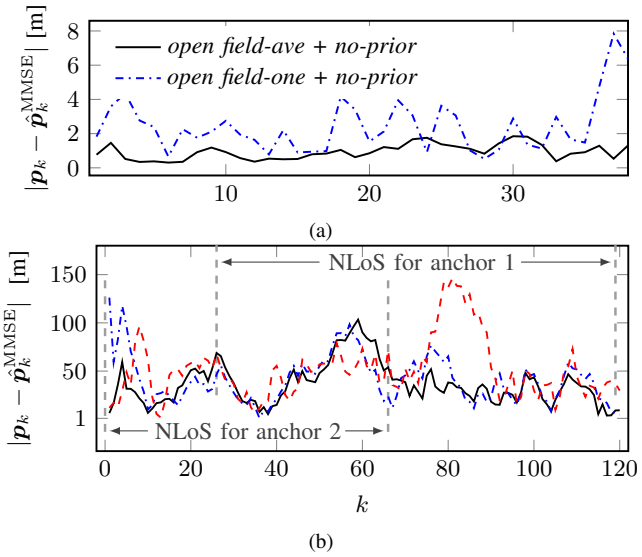

Fig. 8: Target position estimation error: (a) open field datasets; (b) urban datasets: *urban-ave* + *noisy-prior* (——), *urban-ave* + *no-prior* (——), *urban-one* + *noisy-prior* (——). NLoS domains for anchors are denoted with gray dashed lines.

averaging. as shown in Fig. 6. The root mean square position error (RMSE) of the target is 1 m for *open field-ave* and 2.9 m for *open field-one*. The urban scenario is quite challenging, because during the whole measurement time, it is NLoS propagation from the target to one or both anchors. However, the anchors are placed on the high buildings, if the signal is received via roof diffraction, the information of target direction still remains. The target's RMSE is 42 m for *urban-ave* + *noisy-prior*, 47.5 m for *urban-ave* + *no-prior*. Given the most challenging scenario, i.e., *urban-one*, 59.5 m RMSE is achieved with a noisy prior, meaning that real-time outdoor target tracking is possible with RSSD measurements using the proposed framework.

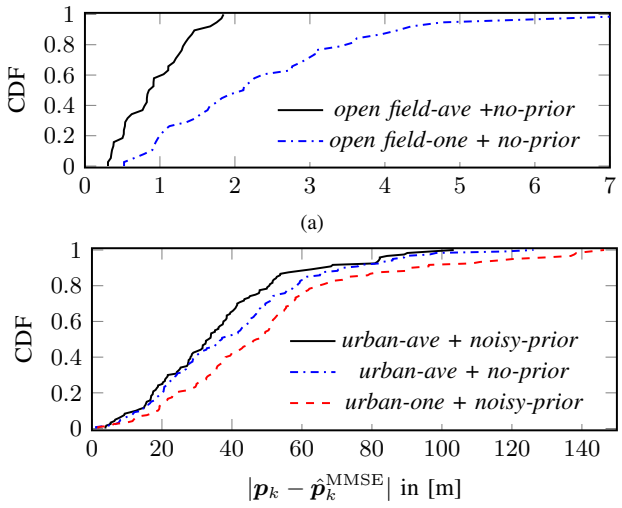

Fig. 9: Empirical CDFs of the position estimation errors: (a) open field datasets; (b) urban datasets.

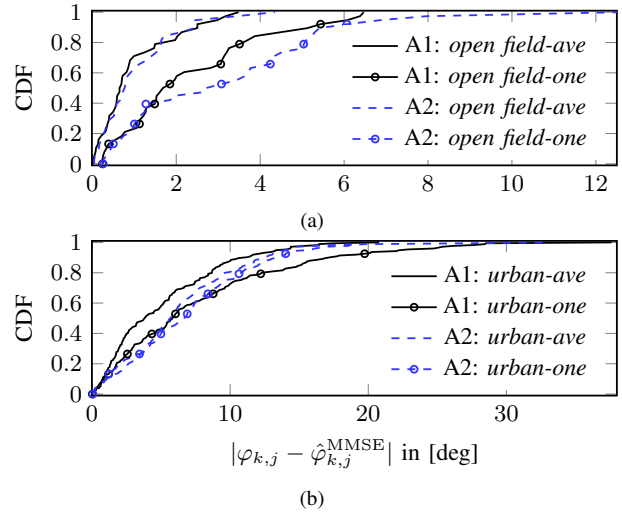

Fig. 10: Empirical CDFs of the AoA estimation errors. (a) open field datasets; (b) urban datasets. Anchor 1 and 2 are abbreviated to A1 and A2.

2) AoA estimation: Empirical CDFs of AoA estimation errors are shown in Fig. 10. It can be observed that anchor 2 achieves similar performance as anchor 1 for all datasets, even with fewer RSSD measurements. Using *open field-ave* dataset, 90% of AoA estimation errors are smaller than 2°, and it increases to 5° when there is no sample averaging (*open field-one*). As shown in Fig. 10b, 90% of errors are smaller than 11° when using *urban-ave*, and 19° when using *urban-one*. It means that for long-range and NLoS propagation conditions, AoA estimates with reasonable accuracy are feasible with the proposed framework. However, averaging over RSS samples did not show significant improvements of the estimates in our case.

V. Conclusion

We proposed an RSSD-based target-tracking/AoA-estimation algorithm for outdoor IoT scenarios. Given known antenna patterns and antenna array geometries, the RSSD model provides direct mapping between AoAs and RSSD measurements, without involving transmit power, path-loss coefficient, phase coherent arrays, etc. Experimental results using LoRaWAN based outdoor measurements show that the proposed framework is able to perform real-time target tracking with reasonable accuracy even without RSS measurements averaging and under NLoS propagation conditions. The AoA estimates can potentially be fused with range estimates to enhance localization. In summary, the proposed framework has very low computational complexity, and is compatible with existing low cost IoT technologies and with different antenna array configurations.

VI. Acknowledgment

This work was supported in part by the Swedish Research Council (VR), in part by the strategic research area ELLIIT.

References

[1] M. Centenaro, L. Vangelista, A. Zanella, and M. Zorzi, "Long-range communications in unlicensed bands: the rising stars in the IoT and smart city scenarios," *IEEE Wirel. Commun.*, vol. 23, no. 5, pp. 60–67, Oct. 2016.

[2] S. Yiu, M. Dashti, H. Claussen, and F. Perez-Cruz, "Wireless RSSI fingerprinting localization," *Signal Process.*, vol. 131, pp. 235 – 244, 2017.

[3] H. Sallouha, A. Chiumento, S. Rajendran, and S. Pollin, "Localization in ultra narrow band IoT networks: Design Guidelines and Trade-Offs," *CoRR*, vol. abs/1907.11205, 2019. [Online]. Available: http://arxiv.org/abs/1907.11205

[4] S. Tomic, M. Beko, and R. Dinis, "RSS-based localization in wireless sensor networks using convex relaxation: Noncooperative and cooperative schemes," *IEEE Trans. Veh. Technol.*, vol. 64, no. 5, pp. 2037–2050, May. 2015.

[5] A. Zanella, "Best practice in RSS measurements and ranging," *IEEE Commun. Surveys Tuts.*, vol. 18, no. 4, pp. 2662–2686, 2016.

[6] N. Podevijn, D. Plets, J. Trogh, L. Martens, P. Suanet, K. Hendrikse, and W. Joseph, "TDoA-based outdoor positioning with tracking algorithm in a public LoRa network," *Wirel. Commun. & Mobile Comput.*, p. 9, 2018. [Online]. Available: http://dx.doi.org/10.1155/2018/1864209

[7] "LoRa alliance geolocation whitepaper," *LoRa Alliance*, 2018. [Online]. Available: https://lora-alliance.org/resource-hub/lora-alliance-geolocation-whitepaper

[8] Z. Jia and B. Guan, "Received signal strength difference–based tracking estimation method for arbitrarily moving target in wireless sensor networks," *Int. J. Distrib. Sens. Netw.*, vol. 14, no. 3, 2018. [Online]. Available: https://doi.org/10.1177/1550147718764875

[9] H. Lohrasbipeydeh, T. A. Gulliver, and H. Amindavar, "Blind received signal strength difference based source localization with system parameter errors," *IEEE Trans. Signal Process.*, vol. 62, no. 17, pp. 4516–4531, Sep. 2014.

[10] A. K. M. M. Hossain and W. Soh, "Cramer-Rao bound analysis of localization using signal strength difference as location fingerprint," in *Proc. IEEE INFOCOM*, Mar. 2010, pp. 1–9.

[11] J. Jiang, C. Lin, F. Lin, and S. Huang, "ALRD: AoA localization with RSSI differences of directional antennas for wireless sensor networks," in *Int. Conf. on Inform. Soc. (i-Society 2012)*, Jun. 2012, pp. 304–309.

[12] Y. Bar-Shalom, T. Kirubarajan, and X.-R. Li, *Estimation with Applications to Tracking and Navigation*. New York, NY, USA: Wiley, 2002.

[13] S. Thomas, "Estimation of nonlinear dynamic systems: Theory and applications," Ph.D. dissertation, Linköpings universitet, Feb. 2006.

[14] S. M. Kay, *Fundamentals of Statistical Signal Processing: Estimation Theory*. Upper Saddle River, NJ, USA: Prentice-Hall, Inc., 1993.

[15] M. S. Arulampalam, S. Maskell, N. Gordon, and T. Clapp, "A tutorial on particle filters for online nonlinear/non-Gaussian Bayesian tracking," *IEEE Trans. Signal Process.*, vol. 50, no. 2, pp. 174–188, Feb. 2002.